

Electronic and Magnetic Properties of 1T-TiSe₂ Nanoribbons

H. D. Ozaydin,^{1,*} H. Sahin,² J. Kang,² F. M. Peeters,² and R. T. Senger^{1,†}

¹*Department of Physics, Izmir Institute of Technology, 35430 Izmir, Turkey*

²*Department of Physics, University of Antwerp, Campus Groenenborgerlaan, 2020 Antwerp, Belgium*

(Dated: October 19, 2018)

Motivated by the recent synthesis of single layer TiSe₂, we used state-of-the-art density functional theory calculations, to investigate the structural and electronic properties of zigzag and armchair-edged nanoribbons of this material. Our analysis reveals that, differing from ribbons of other ultra-thin materials such as graphene, TiSe₂ nanoribbons have some distinctive properties. The electronic band gap of the nanoribbons decreases exponentially with the width and vanishes for ribbons wider than 20 Angstroms. For ultranarrow zigzag-edged nanoribbons we find odd-even oscillations in the band gap width, although their band structures show similar features. Moreover, our detailed magnetic-ground-state analysis reveals that zigzag and armchair edged ribbons have nonmagnetic ground states. Passivating the dangling bonds with hydrogen at the edges of the structures influences the band dispersion. Our results shed light on the characteristic properties of T phase nanoribbons of similar crystal structures.

PACS numbers: 62.23.Kn, 71.15.Mb, 73.22.-f, 71.20.-b

I. INTRODUCTION

Following the first experimental demonstration of graphene,¹ two-dimensional (2D) materials have attracted increasing attention both experimentally and theoretically. Especially transition metal dichalcogenides (TMDs)^{2–4} with chemical formula MX₂ (where M is a transition metal atom and X is a chalcogen atom) have been a favored subject. There are also other stoichiometric forms of transition metal dichalcogenides such as titanium trisulfide (TiS₃) that can form monolayer crystals.⁵ TMDs have a special 2D layered structure. Their mono- and few-layered forms offer many opportunities for fundamental and technological research^{6–8} because of their exceptional electronic, mechanical and optical properties.^{9–12} Furthermore, it is well known that various kinds of TMDs such as MoS₂, WS₂, MoSe₂, WSe₂, ReS₂, NbS₂, TiS₂, and TiSe₂ have been synthesized^{2,13–18} and studies have revealed that TMDs exhibit metallic, semimetallic, semiconducting, and even superconducting behavior with different phases such as 1H, 1T and their distorted forms.

The presence of exotic properties in 2D materials, that stemmed from increasing quantum confinement effects, has also motivated researchers to further reduce their dimension and to investigate one-dimensional (1D) nanoribbons. In early studies it was shown that armchair and zigzag graphene nanoribbons (NRs) were semiconductors with an energy gap decreasing with increasing ribbon width.^{19–22} In addition, zigzag graphene nanoribbons (ZGNRs) have ferromagnetically ordered edge states and can display half-metallic behavior when an external electric field is applied.²³ Furthermore, motivated by the potential use of single layer MoS₂ in nanoscale optoelectronic devices, its nanoribbons have been studied intensively.^{24–26} Armchair MoS₂ NRs are direct band gap semiconductors with a nonmagnetic ground state. Unlike GNRs their band gaps do not vary

significantly with the ribbon width.²⁷ However, zigzag MoS₂ NRs are ferromagnetic metals regardless of their width and thickness.²⁸

Despite the comprehensive research on graphene and single layer TMDs, studies on the electronic properties of the group IVB TMDs in the T phase, namely the two-dimensional 1T-MX₂ structures, are sparse. Nevertheless, 1T-TiSe₂^{29–32} is an extensively studied quasi-2D TMD, which has a charge density wave (CDW) state and in condensed matter physics transitions from superconductivity to charge density wave phases has been shown to be very important.^{33,34} However, whether 1T-TiSe₂ is a semimetal or a semiconductor is still an open question.³⁵ Since TiTe₂ is a semimetal with overlapping valence and conduction bands^{36,37} and TiS₂ is a semiconductor with an indirect gap,^{38,39} it can be expected that the band gap of TiSe₂ is smaller or even nonexistent. Note that in the periodic table selenium is in between sulfur and tellurium, and also selenium is less electronegative than sulfur. Therefore, both experimental and theoretical techniques have been used to identify the semiconducting or semimetallic nature of 1T-TiSe₂.^{40–43} Very recently, Peng et al.⁴⁴ grew TiSe₂ ultrathin films on a graphitized SiC(0001) substrate by using molecular beam epitaxy (MBE). Their findings offer important insights into the nature of the charge density wave in TiSe₂, and paved the way for potential applications based on its collective electronic states.⁴⁴ The successful MBE growth of TiSe₂ ultrathin films down to monolayer thickness motivated us to investigate one-dimensional TiSe₂ nanoribbons because of its interesting electronic and physical properties that are essentially related with its low dimensionality and effects due to quantum confinement. The main goal of this study is to find the characteristics of zigzag- and armchair-edged 1T-TiSe₂ nanoribbons.

The paper is organized as follows. Details of the computational methodology are given in Sec. II. The calculated structural and electronic properties of single

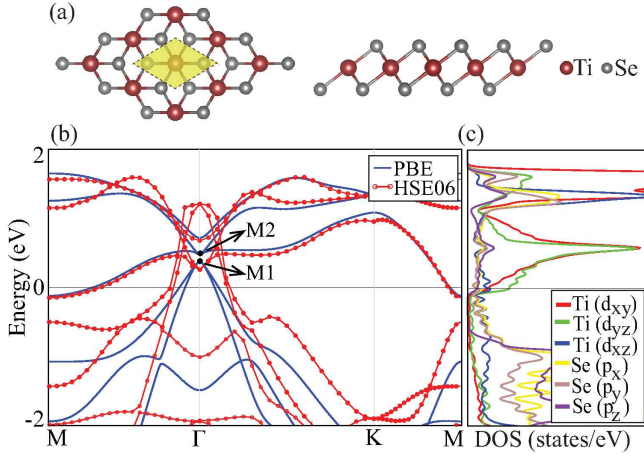


FIG. 1: (Color online) (a) Atomic structure of monolayer 1T-TiSe₂ with top and side views where the dashed yellow area denotes the unitcell of the monolayer, and (b) the band structure calculated with PBE and HSE06, (c) partial density of states as calculated with PBE. Labels M1 and M2 are discussed in Fig. 6.

layer 1T-TiSe₂ are described in Sec. III. Then we analyze 1T-TiSe₂ nanoribbons and present results from spin-unpolarized and spin-polarized calculations in detail in Sec. IV. The last section, Sec. V, is devoted to the conclusion.

II. COMPUTATIONAL METHODOLOGY

The optimized structures and electronic properties of 1T-TiSe₂ nanoribbons with desired edges (zigzag or armchair) reported here are based on first-principle calculations within the density functional theory (DFT) using the plane-wave projector-augmented wave (PAW) method⁴⁵ implemented in the Vienna *ab-initio* simulation package (VASP).^{46–48} The Perdew-Burke-Ernzerhof (PBE)⁴⁹ form of the Generalized Gradient Approximation (GGA) were adopted to describe the electron exchange and correlation for both spin-polarized and spin-unpolarized cases.

In order to correct the PBE band structure for a monolayer of TiSe₂, we also used the Heyd-Scuseria-Ernzerhof 06 (HSE06) functional^{50,51} which is known to give better electronic structure description that is close to experiments and produce accurate band gaps. Since it improves the accuracy of standard band gaps, we determined HSE06 functional parameters as an enhanced fraction of the Hartree-Fock exchange $\alpha = 0.25$ and screening 0.2 \AA^{-1} . The kinetic energy cutoff for the plane-wave expansion was set to 500 eV where the Brillouin Zone (BZ) was sampled with Monkhorst Pack (MP) by $7 \times 1 \times 1$ k-point grids. For all band structure calculations, we used a $75 \times 1 \times 1$ Γ -centered k-point mesh. To avoid the interaction between periodic images, we ensured a sufficient large supercell which is 20 Å long perpendicular to the

nanoribbon plane and with an edge-to-edge distance of at least 13 Å. At the same time, all the atoms in the supercell were fully relaxed during the geometry optimization. The convergence threshold for energy was chosen as 10^{-5} eV and 10^{-4} eV/Å for the force. The charge distribution on the atoms were calculated by using the Bader analysis.^{52,53}

Moreover, we investigated hydrogen saturated nanoribbons in order to study the edge stability. The hydrogen saturation was realized by adding one hydrogen atom to the edge of Ti and Se atoms for the zigzag nanoribbons, however for the armchair nanoribbons one hydrogen atom was added to the edge of Se atoms and two hydrogen atoms are added to the Ti atom. For the determination of the most favorable structure which means the structure after hydrogenation, the binding energies were estimated from: $E_B = E_T[\text{NR}] + nE_T[\text{H}] - E_T[\text{NR} + n\text{H}]$ where $E_T[\text{NR}]$ is the total energy of the TiSe₂ nanoribbon, $E_T[\text{H}]$ is the energy of the free hydrogen atom, $E_T[\text{NR} + n\text{H}]$ is the total energy of the TiSe₂ nanoribbon saturated by hydrogen atoms, and n is the total number of saturated hydrogen atoms.

III. TWO-DIMENSIONAL MONOLAYER TiSe₂

Before a comprehensive investigation of TiSe₂ nanoribbons, we first present the atomic, electronic and magnetic properties of the TiSe₂ monolayer. Principally, layered structures of TMDs can form several different phases, *e.g.* H and T, that result in diverse electronic properties. Monolayer TiSe₂ has a hexagonal crystal structure composed of three atom layers with a metal atom Ti layer sandwiched between two chalcogen Se layers. Here octahedral coordination of the metal atoms results in the 1T structure as shown in Fig. 1(a). Similar to graphite and graphene, in bulk TiSe₂ the monolayers are bound together through the interlayer van der Waals (vdW) interaction. The bond lengths are uniformly $d_{\text{Ti-Se}} = 2.56 \text{ \AA}$, $d_{\text{Se-Se}} = 3.72 \text{ \AA}$, where the angle between the Ti-Se bonds is $\theta_{\text{Se-Ti-Se}} = 93.12^\circ$ and the optimized lattice constant is 3.52 \AA from PBE calculation.

The PBE electronic band dispersion, shown in Fig. 1(b), shows that single layer TiSe₂ is a metal with a non-magnetic ground state. In addition, the partial density of states (PDOS) reveals that while there is negligible contribution from the Se orbitals around the Fermi level (E_F), those bands are mainly composed of Ti-3d orbitals (d_{z^2} , d_{xy} , d_{yz}). At the same time, a Bader analysis indicates that each Ti atom gives 1.4 electrons to the Se atoms which means that 0.7 electrons are taken by one Se atom, hence this situation shows that the character of the bonding is ionic. In contrast, the band structure of 1T TiS₂ is semiconducting. Usually the difference in chalcogen atoms affects the structural properties, but has little influence on the electronic properties. For instance single layers of MoSe₂ and MoS₂ are both direct band gap semiconductors. However, a TiSe₂ sheet exhibits a

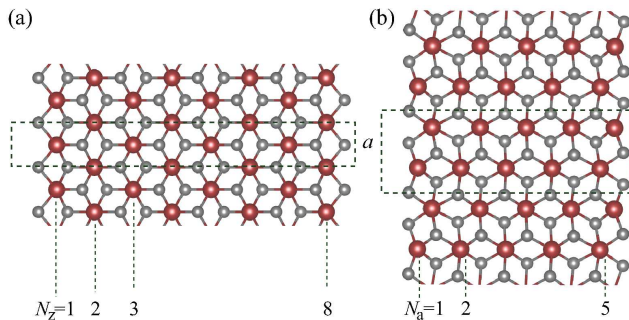


FIG. 2: (Color online) Top view of (a) zigzag and (b) armchair TiSe_2 nanoribbons. The unitcell is indicated by the dashed box.

metallic behavior with a low band crossing of the Fermi level, which is different from TiS_2 .

To further examine the electronic properties of 1T- TiSe_2 , we also calculated the band structure with the HSE06 method which is shown in Fig. 1(b). As can be seen the calculated bands below the Fermi level are shifted upward while above the Fermi level they are slightly shifted downward. At the same time, below the Fermi level the bands are decomposed but the bands above the Fermi level almost overlap with those of the PBE result. In general, relative to the experimental values, band gaps of semiconducting materials are underestimated by PBE. However, PBE+HSE06 provides better agreement with the experimental values. Applying HSE06 corrections to metallic systems is not very common due to its computational cost, and no expected qualitative change in the band structures. Its effect is to introduce some shifts to the bands but the metallic character is preserved. For instance, single-layered VS_2 and T- MoS_2 are still found metallic with HSE06 correction.^{54,55} Consequently, from both the PBE and HSE06 methods we may conclude that TiSe_2 is metallic.

IV. NANORIBBONS OF 1T- TiSe_2

A. Structural Properties

The TiSe_2 nanoribbons (TiSe_2 -NRs) are obtained by cutting the 2D- TiSe_2 monolayer. According to the different directions of termination, there are two kinds of nanoribbons: zigzag (TiSe_2 -ZNR), and armchair (TiSe_2 -ANR). Apart from the termination, TiSe_2 -NRs are defined by their widths. The width of the zigzag nanoribbon is denoted as N_z (TiSe_2 - N_z ZNR) and for armchair nanoribbon, the width is denoted by N_a (TiSe_2 - N_a ANR). In Fig. 2 the lattice structure of TiSe_2 -8ZNR and TiSe_2 -5ANR are presented. In our calculations, we consider width N_z from 2 to 10 and N_a from 2 to 8.

The fully optimized NRs exhibit structural deviation at the edges. For example TiSe_2 -ANRs are strongly distorted after relaxation, compared to TiSe_2 -ZNRs. In the

triple layer networks, the edge selenium atoms shift their position from the Se layers to the Ti layer for both zigzag and armchair nanoribbons whereas the Ti atoms at the edges shift their position from the Ti layer to the Se layers for only zigzag nanoribbons. At one of the edges the Ti atom is closer to the lower Se layer, and the Ti atom at the other edge is closer to the upper Se layer. As seen in Fig. 2(b) for armchair nanoribbons reconstruction takes place, as the Ti atoms at the edges moved towards the ribbon's center and the Se atoms tend to shift slightly outward. For TiSe_2 -8ZNR, shown in Fig. 2(a), the Ti atoms moved slightly out of the plane, leading to a change of the Ti-Se bond length along the ribbon-axis. Nevertheless, the triple-layer networks are well kept intact for both ribbons. For instance, the average Ti-Se bond lengths for TiSe_2 -7ZNR are 2.56 Å in the inner site, and 2.44 Å at the two edges. The angle between Se-Ti-Se bond is 6.22° between the center and edge of the $N_z=7$ zigzag nanoribbon. For the TiSe_2 -8ANR, coordination of atoms are different so that the Ti-Se bond length is different with values of 2.50, 2.57, and 2.64 Å in the inner site, at the edges it decreases to 2.38 Å. All of the nanoribbons display the same structural property, and the only difference is that the bond lengths between the edge Ti-Se atoms are longer in ZNRs than those in ANRs. Similar to the case of MoS_2 nanoribbons,²⁸ at the edges the Ti-Se bond lengths decrease because of the irregular force on the edge atoms. Also, a Bader charge analysis tells us that charges on both Ti and Se atoms are equally distributed along the ribbon axis, since all of the Ti atoms lose the same amount of electron charge which is taken by the Se atoms. Likewise in the 2D- TiSe_2 layer, every Ti atom loses 1.4 electrons to the Se atoms which gain 0.7 electrons along the ribbon axis.

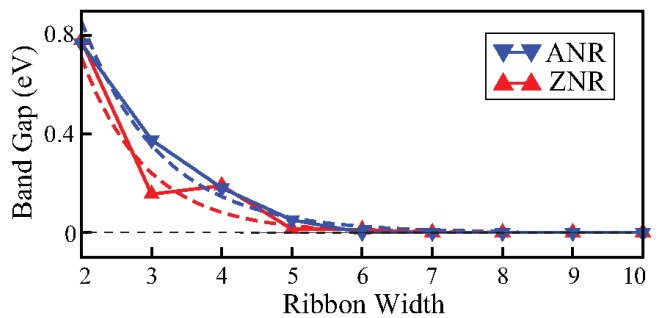


FIG. 3: (Color online) Energy gap of zigzag ($2 \leq N_z \leq 10$) and armchair ($2 \leq N_a \leq 10$) 1T- TiSe_2 nanoribbons as function of the ribbon width. Dashed curves are exponential fits.

B. Electronic Properties

During the geometry optimization, we first carried out both spin-polarized and spin-unpolarized total energy calculations in order to determine the ground state of the different TiSe_2 - N_z ZNR (TiSe_2 - N_a ANR). There is

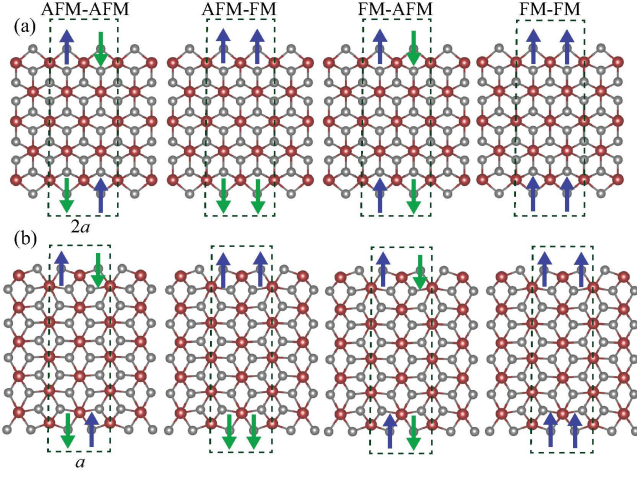


FIG. 4: (Color online) Different magnetic interaction cases for (a) TiSe_2 -5ZNR and (b) TiSe_2 -5ANR.

no energy difference between spin-polarized and spin-unpolarized calculations which indicates that zigzag and armchair TiSe_2 nanoribbons have a nonmagnetic ground state. To be more confident about the magnetization of the edges, we also performed calculations for four different magnetic orderings for TiSe_2 -4ZNR and also TiSe_2 -5ZNR by taking a double unitcell, such as antiferromagnetic (AFM), ferromagnetic (FM) (where, the atoms are located at different edges are AFM coupled, and at the same edge are FM coupled) (see Fig. 4(a)). We take the case of a TiSe_2 -5ZNR as an example. Calculations starting from the four magnetic states, namely AFM-AFM, AFM-FM, FM-AFM, and FM-FM, and results in the same total energy. The same magnetic test is also applied to armchair nanoribbons (see Fig. 4(b)). All the test results gave the same total energy and zero net magnetic moment. As a result, TiSe_2 armchair nanoribbons have a nonmagnetic ground state like MoS_2 -ANRs.²⁸ Thus, our calculation demonstrates that TiSe_2 -ZNRs and TiSe_2 -ANRs are not magnetic and the edge states do not effect the magnetization of the structures.

After analyzing the structural and magnetic properties, we investigated the band dispersion of the TiSe_2 -NRs. Electronic structures of TiSe_2 -NRs show similar behavior like the single-layer 1T- TiSe_2 . In fact, we found that reducing the dimensionality from 2D to 1D, at a certain ribbon width a metal to semiconductor transition is found for both zigzag and armchair nanoribbons as seen in Fig. 3. The band gap decays monotonically with the ribbon width for armchair nanoribbons, however for zigzag nanoribbons the rapid band gap decrease is superposed with an even-odd oscillation with increasing N_z and finally both structures switches to the zero energy gap of monolayer TiSe_2 (for $N_z \geq 7$, and $N_a \geq 6$). Similar oscillatory behavior is also observed in the equilibrium lattice constant for TiSe_2 - N_z ZNRs, when we increase the ribbon width N_z , the lattice constant approached slowly the value 3.52\AA which is the same as that calculated for

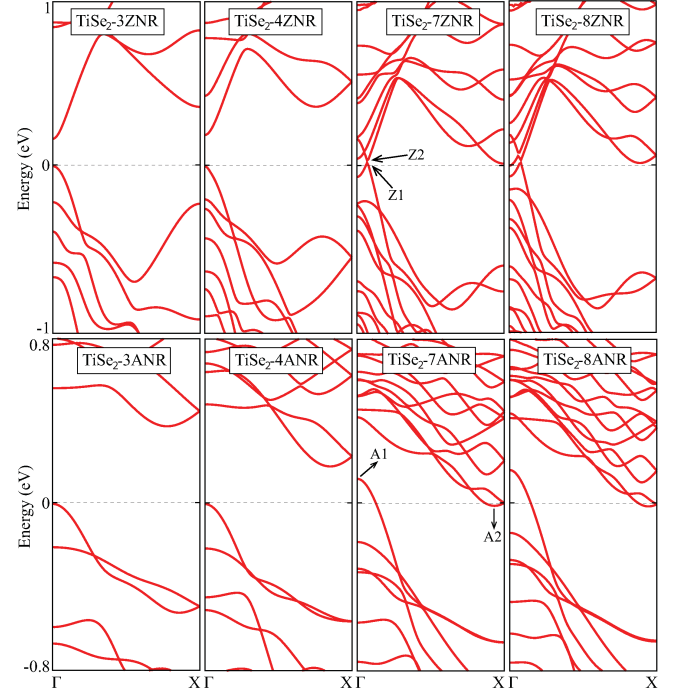


FIG. 5: (Color online) Electronic band structure of a series of zigzag and armchair nanoribbons of 1T- TiSe_2 by using the PBE method.

the 2D- TiSe_2 . The edge reconstructions are more effective in changing the equilibrium lattice constant of ultra narrow ribbons.

As illustrated in Fig. 3, the band gaps as a function of ribbon width for both zigzag and armchair-edged nanoribbons decay very rapidly, except for a small superposed oscillation observed in ultranarrow zigzag nanoribbons. Similar band gap oscillations as a function of ribbon width were also predicted for other semiconducting nanoribbons.²³ Nevertheless, due to the rapid decay in both types of nanoribbons, to provide a quantitative measure for these decays the band gap variations are fitted to the exponential functions, $E_{\text{gap}}(N) = \alpha \exp(-N/\beta)$, where N is the width of the nanoribbon (for ZNRs $N=N_z$ and for ANRs $N=N_a$), and α and β are fitting parameters. For armchair and zigzag nanoribbons, the values of the fitting parameters are found to be $\alpha=5.06$, $\beta=0.89$ eV and $\alpha=6.17$, $\beta=1.08$ eV, respectively. For $N \geq 7$, both types of nanoribbons show metallic behavior.

Spin-unpolarized band structures of TiSe_2 - N_z ZNRs are presented in Fig. 5. Notice that the band structures show similar property at the X-point for odd and even numbers of ribbon width. For the ribbon width of $N_z=2$ a large gap of about 0.786 eV is found. Among the four ZNRs in Fig. 5, TiSe_2 -4ZNR has the largest band gap of 0.201 eV, TiSe_2 -3ZNR has a medium band gap of 0.165 eV, TiSe_2 -5ZNR and TiSe_2 -6ZNR have the smallest band gaps of 12 meV and 5 meV, respectively. Both the direct band gap of zigzag-edged and the indirect band gap of armchair-edged ultranarrow nanoribbons decrease

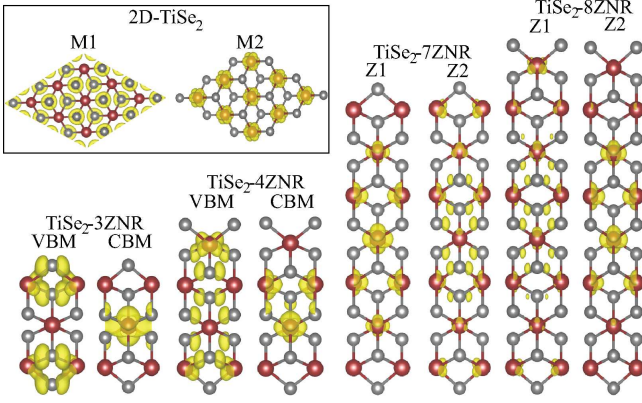


FIG. 6: (Color online) Band decomposed charge density plots of monolayer and $N_z=3,4,7,8$ nanoribbons of TiSe_2 where Z1 and Z2 are shown in the band-structures (see Fig. 5). Inset shows the Γ -point charge densities of M1 and M2 band edges (shown in Fig. 1) of 2D TiSe_2 .

with increasing ribbon width and eventually vanish for $N_z \geq 7$, and $N_a \geq 6$. The conduction band minimum (CBM) and the valance band maximum (VBM) cross resulting in a semimetallic band structure with overlapping bands.

In order to investigate this width-dependent transition in the band structure, as well as the odd-even variations observed in the narrowest ZNRs, we have considered partial charge density (PCD) profiles corresponding to VBM and CBM, or for some specific pair of points in the band structures. These pair of points are M1 and M2 for 2D- TiSe_2 (Fig. 1), Z1 and Z2 for ZNRs, and A1 and A2 for ANRs (Fig. 5). The PCD plots of the VBM and the CBM as shown in Fig. 6 indicate the electronic states around the Fermi level. For TiSe_2 -3ZNR (TiSe_2 -4ZNR), the VBM and the CBM originate from a hybridized mixture of 3d electrons of Ti and 4p electrons of Se atoms with the hybridization being stronger in the VBM than that in the CBM. A comparison of the VBM states of TiSe_2 -3ZNR and TiSe_2 -4ZNR indicate that they are localized more at the edges for odd N_z , whereas they are more uniform distributed for even N_z ribbons. For wider ribbons ($N_z > 4$), both the VBM and CBM states tend to delocalize and the metallic character is attained (this is evident for $N_z=7$ and $N_z=8$ in Fig. 6). With increasing N_z , the PCD plots at the Z1 and Z2 points tend to converge to those at the M1 and M2 pair for 2D- TiSe_2 , where the corresponding states are localized on the Se and Ti atoms, respectively. The opening of a band gap in very narrow ribbons can be attributed to quantum size effects.

Typical band structures for a series of armchair TiSe_2 nanoribbons are also shown in Fig. 5. Unlike zigzag nanoribbons, the electronic structure of the armchair ribbons exhibit an indirect band gap for $N_a \leq 6$. The gap decreases exponentially with the ribbon width. The band gap is almost halved when the ribbon width is increased

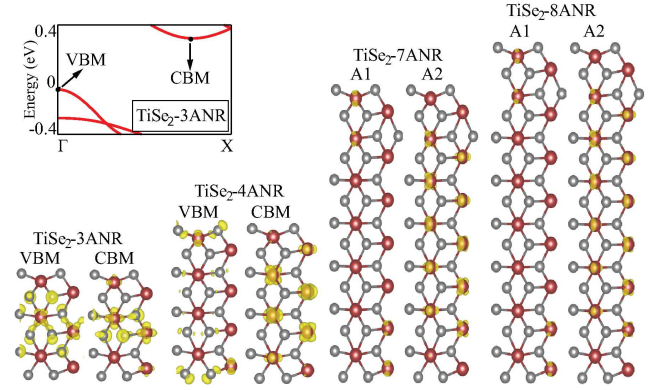


FIG. 7: (Color online) TiSe_2 -3ANR band structure and band decomposed charge densities of $N_a=3,4,7,8$ nanoribbons of TiSe_2 where the A1 and A2 refer to the states indicated in Fig. 5.

from $N_a=2$ to $N_a=4$. TiSe_2 -5ANR still has a band gap of about 5.2 meV. Starting with $N_a=6$, the CBM dips into the Fermi level, so that the armchair nanoribbons become metallic for wider widths. Some partial charge density plots for TiSe_2 - N_a ANRs are also illustrated in Fig. 7. Similarly, the VBM and CBM states are composed of a hybridized mixture of Ti-3d and Se-4p orbitals for small nanoribbons, however for the ribbon width larger than four, the hybridization becomes lost.

V. HYDROGEN TERMINATION OF EDGES

In order to investigate the effect of dangling states present at the edges of the nanoribbons, we have passivated the edge atoms by hydrogen atoms. These unsaturated bonds influence the electronic properties of the ribbons. Naturally these states do not exist in the infinite TiSe_2 single layer, therefore reducing dimensionality from 2D to 1D it will be of importance control the dangling bonds. Earlier, it was shown for graphene nanoribbons that when the dangling bonds at the edges are passivated with hydrogen atoms the electronic and magnetic properties of the ribbons are modified.²² Unlike graphene, the TiSe_2 -NRs have two types of atoms at the edges so that both Ti and Se atoms have to be passivated by hydrogen atoms to compensate the edge states.

Among possible configurations for the edge termination with hydrogen atoms, the most energetically favorable structure is shown for the TiSe_2 -4ZNR in Fig. 8. As seen in the figure where the edge atoms are passivated by hydrogen atoms symmetrically, hydrogenation of the nanoribbons also enhances the stability of the structures. After hydrogenation the ground state energies is lowered, and the binding energy is found to be 11.7 eV for the case of TiSe_2 -4ZNR. The band structures for several hydrogenated ZNRs are shown in Fig. 9. The TiSe_2 - N_z ZNRs are all metallic except for $N_z=4$.

We performed a analysis for the armchair nanoribbons.

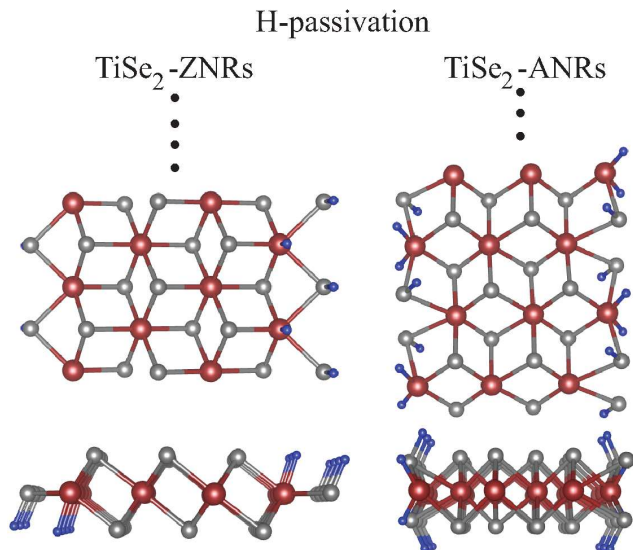


FIG. 8: (Color online) Passivation of the edge states with hydrogen atoms (blue colored) for the zigzag and armchair nanoribbons.

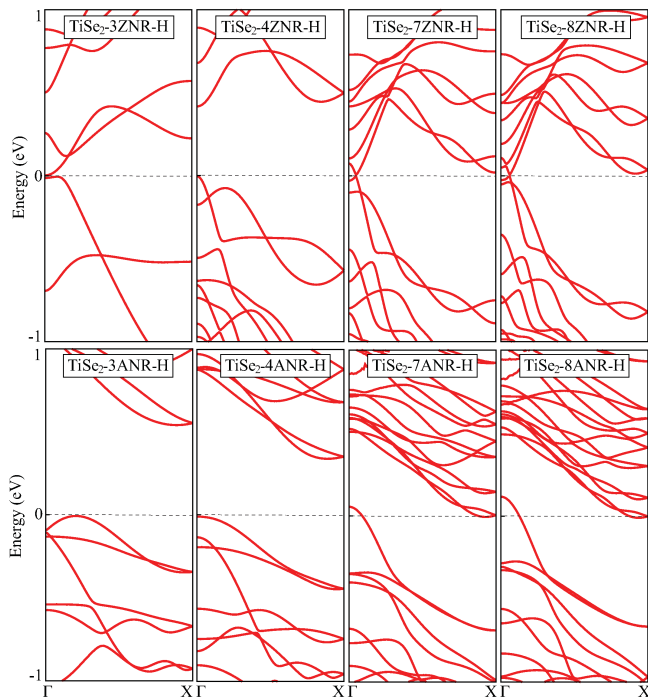


FIG. 9: (Color online) Band structures for zigzag and armchair nanoribbons where the edge atoms are passivated by hydrogen atoms.

In TiSe_2 -3ANR, as an example shown in Fig. 8, the edge Se and Ti atoms are passivated by one and two hydrogen atoms, respectively. The binding energy of the TiSe_2 -3ANR is 23.4 eV. After the hydrogenation, TiSe_2 -3ANR and TiSe_2 -4ANR are semiconductors with an increasing band gap. Also, the VBM state moves a little away from the Γ -point in case of $N_a=3$. TiSe_2 -7ANR and TiSe_2 -8ANR are still metallic after hydrogenation, however the overlap of the conduction and valance bands is reduced.

VI. CONCLUSIONS

In this work, we have investigated the electronic and magnetic properties of zigzag and armchair-edged TiSe_2 nanoribbons by means of first-principles calculations. Overall, our results demonstrate that these TMD nanoribbons which are in 1T phase have quite different characteristics from nanoribbons of other widely studied materials such as graphene or MoS_2 . Our calculations revealed that only ultranarrow zigzag and armchair nanoribbons exhibit semiconducting behavior and their band gap rapidly decreases to zero with increasing ribbon width. $N_a \geq 6$ and $N_z \geq 7$ nanoribbons exhibit metallic behavior like two-dimensional TiSe_2 . The width dependency of the band gap can be fairly represented by an exponential decay function. Both zigzag and armchair ribbons have nonmagnetic ground states. In addition, the robust metallic behavior of both zigzag and armchair TiSe_2 nanoribbons remains unaltered even after passivation of the edges by hydrogen atoms. The metallic character of the wider ribbons of TiSe_2 regardless of their edge symmetry is an advantageous property for utilizing them as one-dimensional interconnects of nanoscale circuits.

Acknowledgments

This work was supported by the Flemish Science Foundation (FWO-VI) and the Methusalem foundation of the Flemish government. Computational resources were provided by TUBITAK ULAKBIM, High Performance and Grid Computing Center (TR-Grid e-Infrastructure). HS is supported by a FWO Pegasus Long Marie Curie Fellowship. JK is supported by a FWO Pegasus Short Marie Curie Fellowship. HDO, HS and RTS acknowledge the support from TUBITAK through project 114F397.

* Electronic address: hediyeengun@iyte.edu.tr

† Electronic address: tugrulsenger@iyte.edu.tr

¹ K. S. Novoselov, A. K. Geim, S. V. Morozov, D. Jiang, Y. Zhang, S. V. Dubonos, I. V. Grigorieva, and A. A. Firsov, *Science* **306**, 666 (2004).

² K. S. Novoselov, D. Jiang, F. Schedin, T. J. Booth, V. V. Khotkevich, S. V. Morozov, and A. K. Geim, *Proc. Natl. Acad. Sci. USA* **102**, 10451 (2005).

³ K. S. Novoselov, A. K. Geim, S. V. Morozov, D. Jiang, M. I. Katsnelson, I. V. Grigorieva, S. V. Dubonos, and A. A.

- Firsov, *Nature London* **438**, 197 (2005).
- ⁴ J. N. Coleman, M. Lotya, A. O'Neill, S. D. Bergin, P. J. King, U. Khan, K. Young, A. Gaucher, S. De, R. J. Smith, I. V. Shvets, S. K. Arora, J. J. Boland, J. J. Wang, J. F. Donegan, J. C. Grunlan, G. Moriarty, A. Shmeliov, R. J. Nicholls, J. M. Perkins, E. M. Grievson, K. Theuwissen, D. W. Mc Comb, P. D. Nellist, and V. Nicolosi, *Science* **331**, 568 (2011).
 - ⁵ F. Iyikanat, H. Sahin, R. T. Senger, and F. M. Peeters, Vacancy Formation and Oxidation Characteristics of Single Layer TiS_3 [Just Accepted], DOI: 10.1021/acs.jpcc.5b01562. Published online: April, 28, 2015.
 - ⁶ Q. H. Wang, K. Kalantar-Zadeh, A. Kis, J. N. Coleman, and M. S. Strano, *Nature Nanotech.* **7**, 699 (2012).
 - ⁷ M. Chhowalla, H. S. Shin, G. Eda, L.-J. Li, K. P. Loh, and H. Zhang, *Nat. Chem.* **5**, 263 (2013).
 - ⁸ X. Huang, Z. Zeng, and H. Zhang, *Chem. Soc. Rev.* **42**, 1934 (2013).
 - ⁹ C. Ataca, H. Sahin, and S. Ciraci, *J. Phys. Chem. C* **116**, 8983 (2012).
 - ¹⁰ H. Wang, L. Yu, Y.-H. Lee, Y. Shi, M. L. Chin, L.-J. Li, M. Dubey, J. Kong, and T. Palacios, *Nano Lett.* **12**, 4674 (2012).
 - ¹¹ Y. J. Zhang, J. T. Ye, Y. Matsushashi, and Y. Iwasa, *Nano Lett.* **12**, 1136 (2012).
 - ¹² H. Fang, S. Chuang, T. C. Chang, K. Takei, T. Takahashi, and A. Javey, *Nano Lett.* **12**, 3788 (2012).
 - ¹³ J. S. Ross, P. Klement, A. M. Jones, N. J. Ghimire, J. Yan, D. G. Mandrus, T. Taniguchi, K. Watanabe, K. Kitamura, W. Yao, D. H. Cobden, and X. Xu, *Nature Nanotech.* **9**, 268 (2014).
 - ¹⁴ S. Tongay, J. Zhou, C. Ataca, K. Lo, T. S. Matthews, J. Li, J. C. Grossman, and J. Wu, *Nano Letters* **12**, 5576 (2012).
 - ¹⁵ S. Horzum, H. Sahin, S. Cahangirov, P. Cudazzo, A. Rubio, T. Serin, and F. M. Peeters, *Phys. Rev. B* **87**, 125415 (2013).
 - ¹⁶ H. Sahin, S. Tongay, S. Horzum, W. Fan, J. Zhou, J. Li, J. Wu, and F. M. Peeters, *Phys. Rev. B* **87**, 165409 (2013).
 - ¹⁷ S. Tongay, H. Sahin, C. Ko, A. Luce, W. Fan, K. Liu, J. Zhou, Y.-S. Huang, C.-H. Ho, J. Yan, D. F. Ogletree, S. Aloni, J. Ji, S. Li, J. Li, F. M. Peeters, and J. Wu, *Nature Comm.*, **5** 3252 (2014).
 - ¹⁸ S. Horzum, D. Cakir, J. Suh, S. Tongay, Y.-S. Huang, C.-H. Ho, J. Wu, H. Sahin, and F. M. Peeters, *Phys. Rev. B* **89**, 155433 (2014).
 - ¹⁹ M. Y. Han, B. Özyilmaz, Y. Zhang, and P. Kim, *Phys. Rev. Lett.* **98**, 206805 (2007).
 - ²⁰ D. A. Abanin, P. A. Lee, and L. S. Levitov, *Phys. Rev. Lett.* **96**, 176803 (2006).
 - ²¹ H. Sahin, C. Ataca, and S. Ciraci, *Phys. Rev. B* **81**, 205417 (2010).
 - ²² V. Barone, O. Hod, and G. E. Scuseria, *Nano Lett.* **2748** (2006).
 - ²³ Y.-W. Son, M. L. Cohen, and S. G. Louie, *Nature London* **444**, 347 (2006).
 - ²⁴ Q. Li, E. C. Walter, W. E. van der Veer, B. J. Murray, J. T. Newberg, E. W. Bohannon, J. A. Switzer, J. C. Hemminger, and R. M. Penner, *J. Phys. Chem. B* **109**, 3169 (2005).
 - ²⁵ A. R. Botello-Mendez, F. Lopez-Uras, M. Terrones, and H. Terrones, *Nanotechnology* **20**, 325703 (2009).
 - ²⁶ H. Pan and Y.-W. Zhanga, *J. Mater. Chem.* **22**, 7280 (2012).
 - ²⁷ C. Ataca, H. Sahin, E. Aktürk, and S. Ciraci, *J. Phys. Chem. C* **115**, 3934 (2011).
 - ²⁸ Y. Li, Z. Zhou, S. Zhang, and Z. Chen, *J. Am. Chem. Soc.* **130**, 16739 (2008).
 - ²⁹ F. Di Salvo, D. Moncton, and J. Waszczak, *Phys. Rev. B* **14**, 4321 (1976).
 - ³⁰ C. M. Fang, R. A. de Groot, and C. Haas, *Phys. Rev. B* **8**, 4455 (1997).
 - ³¹ G. Li, W. Z. Hu, D. Qian, D. Hsieh, M. Z. Hasan, E. Morosan, R. J. Cava, and N. L. Wang, *Phys. Rev. Lett.* **99**, 027404 (2007).
 - ³² A. F. Kusmartseva, B. Sipos, H. Berger, L. Forro, and E. Tutis, *Phys. Rev. Lett.* **103**, 236401 (2009).
 - ³³ M. Bovet, D. Popovi, F. Clerc, C. Koitzsch, U. Probst, E. Bucher, H. Berger, D. Naumovi, and P. Aebi, *Phys. Rev. B* **69**, 125117 (2004).
 - ³⁴ E. Morosan, H. W. Zandbergen, B. S. Dennis, J. W. G. Bos, Y. Onose, T. Klimczuk, A. P. Ramirez, N. P. Ong, and R. J. Cava, *Nature Phys.* **2**, 544 (2006).
 - ³⁵ J. C. E. Rasch, T. Stemmler, B. Müller, L. Dudy, and R. Manzke, *Phys. Rev. Lett.* **101**, 237602 (2008).
 - ³⁶ D. K. G. de Boer, C. F. Van Bruggen, G. W. Bus, R. Coehoorn, C. Haas, G. A. Sawatzky, H. W. Myron, D. Norman, and H. Padmore, *Phys. Rev. B* **29**, 6797 (1984).
 - ³⁷ R. Claessen, R. O. Anderson, G.H. Gweon, J. W. Allen, W. P. Ellis, C. Janowitz, C. G. Olson, Z. X. Shen, V. Eyert, M. Skibowski, K. Friemelt, E. Bucher, and S. Hüfner, *Phys. Rev. B* **54**, 2453 (1996).
 - ³⁸ C. H. Chen, W. Fabian, F. C. Brown, K. C. Woo, B. Davies, B. DeLong, and A. H. Thompson, *Phys. Rev. B* **21**, 615 (1980).
 - ³⁹ D. Samulsen, E. Pehlke, W. Schattke, O. Anderson, R. Manzke, and M. Skibowski, *Phys. Rev. Lett.* **68**, 522 (1992).
 - ⁴⁰ T. Pillo, J. Hayoz, H. Berger, F. Levy, L. Schlapbach, and P. Aebi, *Phys. Rev. B* **61**, 16213 (2000).
 - ⁴¹ M. Calandra and F. Mauri, *Phys. Rev. Lett.* **106**, 196406 (2011).
 - ⁴² B. Hildebrand, C. Didiot, A. M. Novello, G. Monney, and A. Scarfato, *Phys. Rev. Lett.* **112**, 197001 (2014).
 - ⁴³ M. Rösner, S. Haas, and T. O. Wehling, *Phys. Rev. B* **90**, 245105 (2014).
 - ⁴⁴ J.-P. Peng, J.-Q. Guan, H.-M. Zhang, and C.-L. Song, *Phys. Rev. B* **91**, 12113 (2015).
 - ⁴⁵ P. E. Blöchl, *Phys. Rev. B* **50**, 17953 (1994).
 - ⁴⁶ G. Kresse and J. Furthmüller, *J. Phys. Rev. B* **47**, 558 (1993).
 - ⁴⁷ G. Kresse and J. Furthmüller, *Comp. Mat. Sci.* **6**, 15 (1996); *Phys. Rev. B* **54**, 11169 (1996).
 - ⁴⁸ G. Kresse and D. Joubert, *Phys. Rev. B* **59**, 1758 (1999).
 - ⁴⁹ J. P. Perdew, K. Burke, and M. Ernzerhof, *Phys. Rev. Lett.* **77**, 3865 (1996).
 - ⁵⁰ J. Heyd, G. R. Scuseria, and M. Ernzerhof, *J. Chem. Phys.* **118**, 8207 (2003).
 - ⁵¹ J. Heyd, G. R. Scuseria, and M. Ernzerhof, *J. Chem. Phys.* **124**, 219906 (2006).
 - ⁵² R. F. W. Bader, *Atoms in Molecules - A Quantum Theory*, (Oxford University Press, Oxford, 1990).
 - ⁵³ G. Henkelman, A. Arnaldsson, and H. Johnson, *Comput. Mater. Sci.* **36**, 354 (2006).
 - ⁵⁴ J. Feng, X. Sun, C. Wu, L. Peng, C. Lin, S. Hu, J. Yang, and Yi Xie, *J. Am. Chem. Soc.* **133**, 17832 (2011).
 - ⁵⁵ M. Kan, J. Y. Wang, X. W. Li, S. H. Zhang, Y. W. Li, Y.

Kawazoe, Q. Sun, and P. Jena, J. Chem. Phys. **118**, 1515 (2014).